Proceedings of ASME Turbo Expo 2011
GT2011
June 6-10, 2011, Vancouver, British Columbia, Canada

GT2011-46848

STABILITY OF FLEXIBLE ROTORS WITH A LEBLANC BALANCER

Leonardo Urbiola-Soto*
Ph.D. Student,
Department of Mechanical Engineering
Universidad Nacional Autonoma de Mexico
(UNAM) Campus Juriquilla, Queretaro, Mexico
76230
leourbiola@gmail.com

Marcelo Lopez-Parra
Professor
Department of Mechanical Engineering
Universidad Nacional Autonoma de Mexico
(UNAM) Campus Juriquilla, Queretaro, Mexico
76230

ABSTRACT

Although the liquid balancer has nearly a century of having been introduced by LeBlanc, little information is available on the dynamic response and stability behavior of this kind of device. Earlier author's research using a high-speed camera and a Particle Image Velocimetry (PIV) technique showed the existence of a fluid backward traveling wave inside the balancer cavity. This damping phenomenon helps enhance the unbalance response of the rotating system and also raises the stability limits. This paper shows that a flexible rotor employing a LeBlanc balancer has remarkable increase in the threshold speed of instability for aerodynamic cross-coupling and viscous internal friction damping.

NOMENCLATURE

c Damping, N·s/m
$d = z\, r_f^2/(r_o^2 - r_f^2)$ Distance from **C** to **F**, m
k Stiffness, N/m
h Balance ring height, m
$f = \omega/\omega_{cr}$ Frequency ratio, dimensionless
$j = \sqrt{-1}$ Imaginary unit, dimensionless
m,n Circumferential and lateral modes of vibration
m Mass, kg
r radius, m
x,y Cartesian coordinates, m
$\bar{z} = z\, r_o^2/(r_o^2 - r_f^2)$ Distance from **O** to **F**, m
C Disk center
F Fluid center of gravity
M Disk center of gravity
O Bearing center
$q = c_i\omega$ Aerodynamic cross-coupling coefficient, N/m
$\mathbf{z} = x + jy$ Complex disk motion, m
$\mathbf{z_1} = x_1 + jy_1$ Complex journal motion, m
$K = k_1/k_r$ Stiffness ratio, dimensionless
$M = m_f/m_r$ Total fluid mass ratio, dimensionless
$M_b = m_b/m_r$ Backward traveling wave mass ratio, dim'less
β Unbalance response phase angle, rad
$\xi = c/2\, m_r\omega_{cr}$ Damping ratio, dimensionless
ρ Fluid density kg/ m^3
ω Frequency, rad/s

Subscripts

1 Bearing property
b Fluid traveling backwards property
cr Rotor critical speed on rigid supports, rad/s
d Whirl frequency, rad/s
e Effective property
f Fluid property
i Rotor internal property
i Inner
m Maximum value
o Outer
op Optimum value
r Rotor property

INTRODUCTION

There has been considerable work in the area of the dynamics of rotors with internal damping that is well-documented in the literature, particularly with regard to internal friction arising from micro-slip at shrink-fit interconnections of built-up rotors.

* Corresponding author

Newkirk [1] pointed that internal rotor damping created by shrink fits of impellers and spacers is a predominant cause of whirl instability. Kimball [2] by means of deriving the equations of motion showed that the internal friction force tends to put the shaft motion in an ever-increasing spiral path. Gunter [3] developed a linear rotordynamic model in which internal friction was modeled as a cross-coupled force. He demonstrated that if external damping is added, the threshold speed could be greatly improved. He also showed that foundation asymmetry without foundation damping can cause a large increase of the onset speed of instability. Black [4] investigated a variety of models (viscous, Coulomb and hysteretic) for internal friction and differentiated between various models in reference to their ability to accurately predict the onset of instability. Lund [5] also investigated internal friction models, specifically due to micro-slip at axial splines and shrink fit joints. Srinivasan [6] showed that at some values of low interference fit, the system became unstable at high speeds, while no instability was noted for tighter fits. Damping for the low interference fit was higher than for the high interference. The aforementioned is due to the fact that when the fit is tight, slipping at the interference between the disk and the shaft is reduced. In most cases, the whirl instability can be suppressed with hardware fixes such as changing the bearings to softer supports with asymmetric stiffness, adding more damping in the bearings or tightening the interference fits. This paper proposes an alternative mechanism for improving rotor stability by using a LeBlanc balancer.

The LeBlanc balancer is basically a hollow ring equipped with a number of pockets formed by radial walls and partially filled with liquid. The limited information on this liquid balance ring made public can be found on a number of patents and a few technical papers and thesis work. Back in 1914, LeBlanc [7] first introduced a passive dynamic balancing device for turbine rotors consisting of an annular cavity partially filled with a liquid of high viscosity. However, this kind of device has not received much attention for practical use in turbomachiney since then. It has extensively been demonstrated that when a flexible rotor is partially filled with liquid, the motion is unstable over some operating range [8-11]. The extent of this operating range depends on various system parameters such as rotor damping, stiffness, fluid viscosity, the amount of fluid present, etc. However, when the cavity filled with liquid is provided with a number of radial baffle boards, the unstable behavior changes dramatically, helping the rotating system achieve higher stable operating speeds.

Linear stability analysis is carried out on a balance ring equipped with a number of eight baffles boards and partially filled with a brine solution at a ratio of 0.5. Experimental results reported by Urbiola-Soto and Lopez-Parra [12] on fluid flow visualization and Particle Image Velocimetry (PIV) are used to understand the fluid-solid interaction of the brine solution employed and the balance ring baffles. The onset of unstable dynamic response is examined. Balance ring blades and fluid inertia are found to play an important role in the onset of instability.

EXPERIMENTAL APPARATUS

Fluid flow visualization and PIV experiments were performed on a vertical axis washing machine equipped with a liquid balance ring on top of the rotating drum and running up to 1000 rpm. The test rig experimental settings are fully described in [12]. The balance ring employed mainly consists of an annular cavity of 3.709E-03 m^3 equipped with a number of eight radial baffles equiangularly spaced. Sodium chloride with a density of 1300 kg/m^3 was employed to fill the cavity. Figure 1 shows the balance ring under study consisting of a thermoformed Polyethylene Terephthalate (PET) ring assembled by two parts. The bottom part houses the baffles, which are inserted in machined guiding grooves. The upper part works as a top cover bolted to the bottom portion. The balance ring assembly is rigidly mounted on top of the rotating drum through a set of brackets. Clearances are provided with the inner and outer wall, and also with the top cover. This helps achieve higher order fluid modes of vibration.

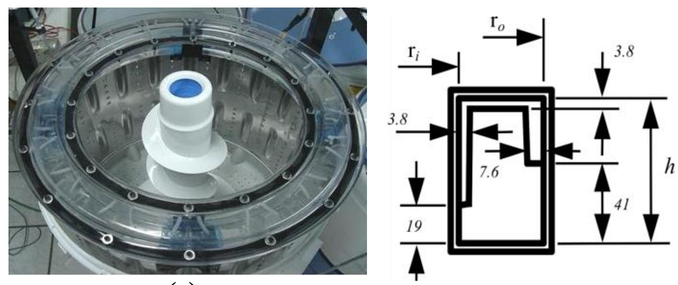

(a) (b)

Figure 1. Transparent balance ring; (a) top view, and (b) radial baffle, dimensions in mm.

A high-speed camera at 1000 frames/s and a set of white light sources of Xenon lamps type were used for direct fluid flow visualization. A laser beam was orthogonally oriented with respect to the direction of the observing camera by using an articulated arm system.

FLUID FLOW VISUALIZATION AND PIV RESULTS

As reported by Urbiola-Soto and Lopez-Parra [12], the removal of baffles inside the ring rendered a partially wetted cavity as shown on Fig. 2. A strong unstable vibration occurred at speeds as low as 200 rpm, this behavior is similar to trapped fluids (e.g., oil from bearing sumps, steam condensate, etc.) in the internal cavity of high-speed hollow rotors [8]. As explained by [13], the fluid does not remain in simple radial orientation. The spinning surface of the cavity drags the fluid (which has some finite viscosity) in the direction of rotation. This fluid shear stress results in a tangential force in the direction of rotation. This force is called follower force and is the fundamental condition for instability. On the contrary, the addition of baffles showed that the fluid is not stationary relative to the rigid body, see Fig. 3. Furthermore, the baffles increased the natural frequency of the fluid and induced a complex fluid mode of vibration. The experimental rig was always stable at speeds as high as 1000 rpm once the baffles were put in place inside the ring.

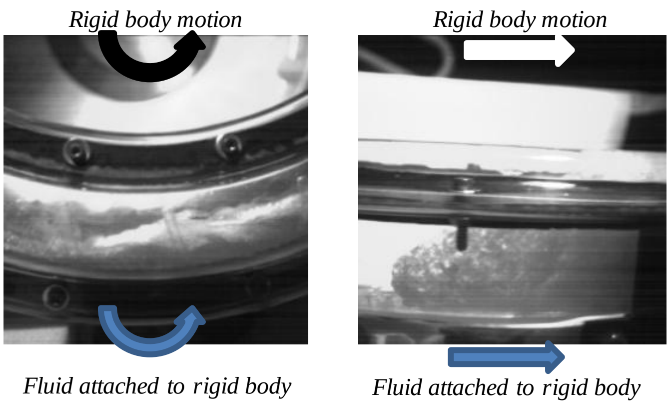

(a) (b)

Figure 2. Fluid bulk-flow in a hollow ring with no baffles; (a) top view, and (b) side view.

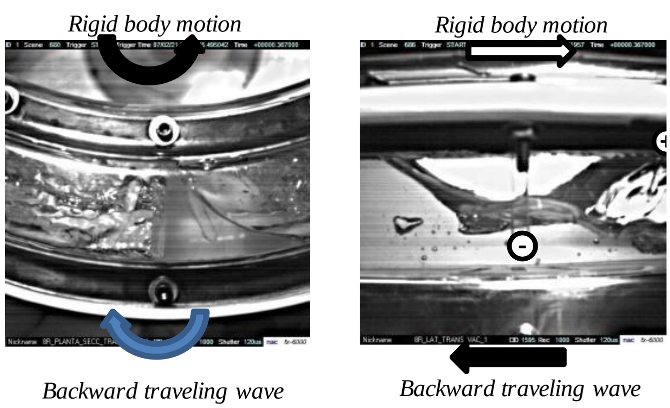

(a) (b)

Figure 3. Backward traveling wave, (a) top view, and (b) side view, (+) and (-) indicate a crest and valley, respectively.

As shown on Fig. 1(b) the radial baffles placed in the cavity account with gaps with the inner and outer walls, this enables a backward traveling fluid wave that describes a swirl at low speeds, Fig. 3(b). As the speed increases, the fluid motion occurs throughout the liquid interior and is thus called an internal wave or inertia oscillation [14]. The stability mechanism is due to this backward traveling wave present in the fluid, which acts as an added damping force. The fluid mass of such wave has been found to be a fraction of the total fluid mass and synchronous with the rotor speed [12].

The motion in the rotating body is transmitted to the contacting liquid by shear stress; this suggests that waves are occurring in the fluid. Since the spin axis does not coincide with the angular momentum vector, the drum rotor appears to oscillate about its transverse x and y axes. This oscillation or whirling causes the liquid in the ring to move relative to the rigid body. If the drum rotor spins about a major moment-of-inertia axis, the liquid motions tend to damp the whirling. The energy dissipated by the oscillatory motions is extremely large when the whirling motion excites the liquid into resonance. This motion does not relate to free surface sloshing. In fact, the motion occurs throughout the liquid interior and is thus called an internal wave or inertia oscillation [14]. Urbiola-Soto and Lopez-Parra [12] used Miles and Troesch [14] three-dimensional equations to compute the oscillating fluid frequency for a balance ring with 8 baffles boards exciting fluid coupled vibrating modes; m = *4* and n = *8*. They showed analytically and experimentally that the backward traveling wave is synchronous with the rotor running frequency. The fluid relative velocity map was built by superposition of PIV frames for different portions of the balance ring as illustrated on Fig. 4. This mass induces a tangential force 90^o phase lagged with the solid body motion, thus behaving as a positive damping stabilizing effect. The effective mass (m_b) traveling backwards is a fraction of the total fluid mass given by Eq. (1)

$$15^\circ \times 8 \;\; \mathit{HighRelative\,Velocity\,Zones} = 120^\circ = \frac{1}{3}\mathit{Circumference} \qquad (1)$$

Therefore, the effective "fluid damping mass" is one third of the total fluid mass

$$m_b = 0.33 \;\; m_f \qquad (2)$$

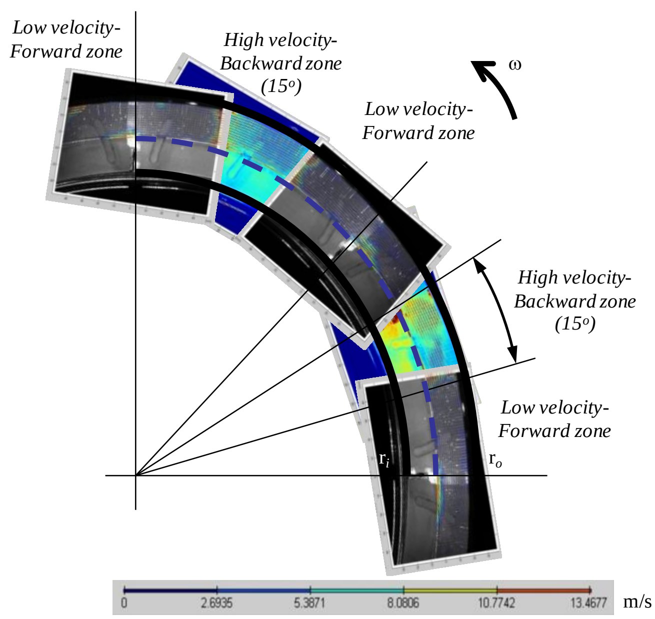

Figure 4. Balance ring relative velocity map.

UNBALANCE RESPONSE

Figure 5 provides a 2-dof dynamic model of a flexible rotor in flexible symmetric damped bearings and with a LeBlanc balancer. It has been assumed that the bearings cross-coupled stiffness and damping coefficients are negligible as might be the case of tilting pad journal bearings and squeeze film dampers. Thus bearings are not considered to be a source of instability in this analysis. Furthermore, for the sake of simplicity, the bearings are assumed to be essentially identical and symmetric.

Then, for the flexible rotor, the differential equations of motion of the rotor are given by

$$m_r\ddot{\boldsymbol{z}} + k_r\left(\boldsymbol{z} - \boldsymbol{z}_1\right) + m_f\,\bar{\boldsymbol{z}}\omega^2 + 2m_b\dot{\boldsymbol{d}}\omega = m_r u\omega^2 e^{j\omega t} \quad (3)$$

$$k_1\boldsymbol{z}_1 + k_r\left(\boldsymbol{z}_1 - \boldsymbol{z}\right) + c_1\dot{\boldsymbol{z}}_1 = 0 \quad (4)$$

Eqs. (3) and (4) are combined to give

$$\ddot{\boldsymbol{z}} + 2\omega_{cr}\xi_e\dot{\boldsymbol{z}} + 2\mathrm{M}_b\dot{\boldsymbol{d}}\omega + \Omega^2\boldsymbol{z} + \mathrm{M}\bar{\boldsymbol{z}}\omega^2 = u\omega^2 e^{j\omega t} \quad (5)$$

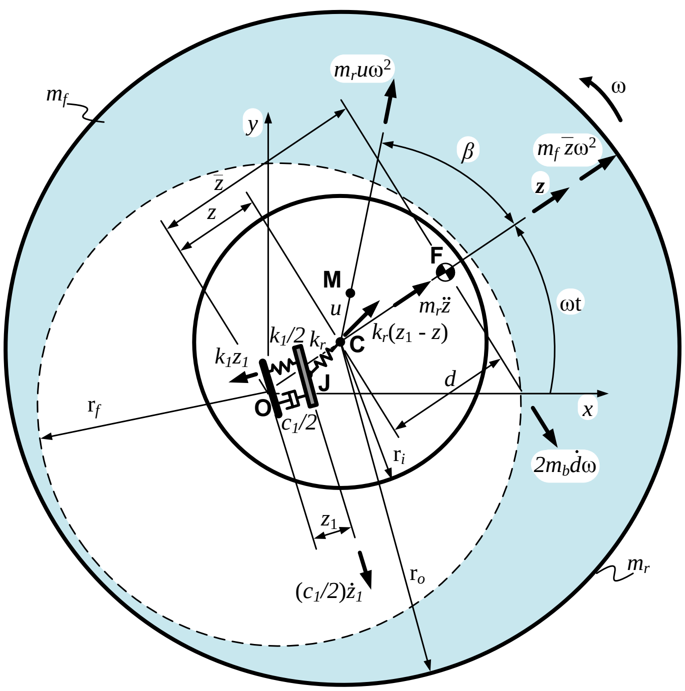

Figure 5. Dynamic model of a flexible rotor with a LeBlanc Balancer.

Note that a damping term $2m_b\dot{\boldsymbol{d}}\omega$ has been added, which can be thought mainly as viscous dissipation in the bulk-flow. In other words, this additional damping is due to the mass fraction moving backwards relative to the rigid body. The acceleration of the backward traveling wave, which mass is m_b, has no radial component and only possesses tangential or Coriolis acceleration given by $2\dot{\boldsymbol{d}}\omega$. Therefore, its tangential force is defined by the term $2m_b\dot{\boldsymbol{d}}\omega$., where the wave frequency is synchronous with ω. Solution of Eqs. (3) and (4) renders

$$z = \frac{u}{\left[\left(\dfrac{\Omega^2}{\omega^2} - 1 + \dfrac{\rho\pi r_o^2 h}{m_r}\right)^2 + \left(2\dfrac{\omega}{\omega_{cr}}\xi_e + 2\mathrm{M}_b\left(\dfrac{\mathrm{r}_f^2}{\mathrm{r}_o^2 - \mathrm{r}_f^2}\right)\right)^2\right]^{1/2}} \quad (6)$$

$$z_1 = \frac{z}{\left[\left(\mathrm{K} + 1 - \mathrm{Mf}^2\right)^2 + \left(2\xi_1\mathrm{f}\right)^2\right]^{1/2}} \quad (7)$$

The phase lag is given by

$$\beta = \tan^{-1}\left|\frac{2\dfrac{\omega}{\omega_{cr}}\xi_e + 2\mathrm{M}_b\left(\dfrac{\mathrm{r}_f^2}{\mathrm{r}_o^2 - \mathrm{r}_f^2}\right)}{\dfrac{\Omega^2}{\omega^2} - 1 + \dfrac{\rho\pi r_o^2 h}{m_r}}\right| \quad (8)$$

Where

$$\Omega^2 = \omega_{cr}^2\left|\frac{\mathrm{K}(\mathrm{K}+1) + (2\mathrm{f}\xi_1)^2}{(\mathrm{K}+1)^2 + (2\mathrm{f}\xi_1)^2}\right| \quad (9)$$

Note that Ω is the rotor critical speed on flexible supports.

$$\xi_e = \frac{\xi_1}{(\mathrm{K}+1)^2 + (2\xi_1\mathrm{f})^2} \quad (10)$$

Gunter *et. al.* [19] has shown that the effective damping can be maximized with respect to the bearing damping by finding the value of ξ_1 which satisfies $\partial\xi_e/\partial\xi_1 = 0$. Hence

$$\xi_{em} = \frac{1}{4(\mathrm{K}+1)} \quad (11)$$

$$\xi_{1op} = \frac{\mathrm{K}+1}{2} \quad (12)$$

The effects of aerodynamic cross-coupling and rotor internal damping will now be considered.

STABILITY WITH OPTIMUM DAMPING AND A LEBLANC BALANCER

Rotor bearing systems are frequently subjected to self-excited instabilities mechanisms including bearings, seals, aerodynamic effects, and internal rotor friction damping. For free damped vibrations with aerodynamic cross-coupling and optimum bearing damping, Eq. (5) becomes

$$\ddot{\boldsymbol{z}} + 2\omega_{cr}\xi_{em}\dot{\boldsymbol{z}} + 2\mathrm{M}_b\dot{\boldsymbol{d}}\omega + (\Omega^2 - j\mathrm{Q})\boldsymbol{z} + \mathrm{M}\bar{\boldsymbol{z}}\omega^2 = u\omega^2 e^{j\omega t} \quad (13)$$

Where ξ_{em} is given by Eq. (11) and Q = q/m_r

$$\Omega_{op}^2 = \omega_{cr}^2\left[\frac{2\mathrm{K}+1}{2(\mathrm{K}+1)}\right] \tag{14}$$

With viscous internal friction damping Eq. (5) becomes

$$\ddot{\boldsymbol{z}} + 2\omega_{cr}(\xi_{em}+\xi_{\mathrm{i}})\dot{\boldsymbol{z}} + 2\mathrm{M}_b\dot{\boldsymbol{d}}\omega + \Omega^2\boldsymbol{z} + \mathrm{M}\bar{\boldsymbol{z}}\omega^2 = u\omega^2 e^{j\omega t} \tag{15}$$

Assuming an exponential function of the form $\boldsymbol{z}$ = ze^{st}, the characteristic equation is of the form

$$m_r s^2 + \left[c_{em} + c_{\mathrm{i}} + 2m_b\omega\left(\frac{\mathrm{r}_f^2}{\mathrm{r}_o^2-\mathrm{r}_f^2}\right)\right]s + \frac{\mathrm{K}(2\mathrm{K}+1)}{2(\mathrm{K}+1)} + m_f\left(\frac{\mathrm{r}_o^2}{\mathrm{r}_o^2-\mathrm{r}_f^2}\right)\omega^2 = 0 \tag{16}$$

The values of s satisfying Eq. (15) are the system eigenvalues. Since s is complex, Eq. (16) represents a complex function. In order to be zero, both the real and imaginary parts must be simultaneously zero. Substituting $s = \lambda + j\omega_d$ into Eq. (16) and equating individually the real and imaginary part to zero results in a pair or polynomial with real coefficients, which need to be solved simultaneously. A rather simple solution for which the rotor becomes unstable can be found by substituting $\lambda = 0$ to deliver

$$\omega_{d\,op} = \left[\omega_{cr}^2\left(\frac{2\mathrm{K}+1}{2(\mathrm{K}+1)}\right) + 2\omega^2\mathrm{M}_b\left(\frac{\mathrm{r}_f^2}{\mathrm{r}_o^2-\mathrm{r}_f^2}\right)\right]^{1/2} \tag{17}$$

Whereas with viscous internal friction damping, the rotor will only be stable if the operating speed is

$$\omega < \Omega_{op}\left[1 + \frac{1}{4(1+\mathrm{K})\xi_{\mathrm{i}}} + \mathrm{M}_b\frac{\mathrm{f}}{\xi_{\mathrm{i}}}\left(\frac{\mathrm{r}_f^2}{\mathrm{r}_o^2-\mathrm{r}_f^2}\right)\right]^{1/2} \tag{18}$$

According to Eq. (17), when the rotor is unstable, it whirls at the undamped natural frequency plus the rising term depending on the traveling backwards mass of the LeBlanc balancer and its geometrical properties as well. On the other hand, Eq. (18) shows that for the rotor to be unstable due to internal friction damping, the rotational speed must exceed the undamped natural frequency plus a destabilizing term depending on the internal friction damping, plus a rising term depending on the traveling backward mass of the LeBlanc balancer and its geometrical properties.

While the maximum permissible aerodynamic cross-coupling with optimum damping is

$$q_{mop} = 2m_r\omega_{cr}\omega_d\left[\xi_{em} + \mathrm{M}_b\frac{\mathrm{f}}{2}\left(\frac{\mathrm{r}_f^2}{\mathrm{r}_o^2-\mathrm{r}_f^2}\right)\right]^{1/2} \tag{19}$$

EXAMPLES

Industrial rotor cases will be taken form reference [15] to analyze the effect of the LeBlanc balancer to improve their stability. The internal damping for those rotors is unknown a priori. Some guessed values for the internal damping will be assumed for two conditions, namely loose and tight fit. The first example is a ten-stage centrifugal compressor, designated in the following as the "light-rotor". The unit is nearly symmetrical and the rotor is supported in two five-pad tilting pad bearings. A second example, considers the seven-stage centrifugal compressor, designated from now on as the 'heavy rotor". This is a rotor mounted on very rigid pressure dam journal bearings with different stiffness values on the horizontal and vertical directions. The third example deals with an eight-stage centrifugal compressor supported on tilting pad journal bearings mounted in series with squeeze film dampers, where the stiffness values on the horizontal and vertical direction differ greatly from each other. The final example is the Space Shuttle Main Engine-High Pressure Fuel Turbopump (SSME-HPFTP). The HPFTP consists of a three-stage centrifugal pump section and a two-stage turbine section as shown in Fig. 6. Details of the pump configuration are given in reference [16]. The rotating assembly is supported in flexible mounted ball bearings and is acted on by aerodynamic cross-coupling forces in the turbine section. For the purpose of analyzing the stabilizing effect of the LeBlanc balancer, it will be assumed that little damping is provided to the rotor from the bearings, supports and seals. The supports will be considered symmetric and isotropic. Different bearing stiffness values will be considered.

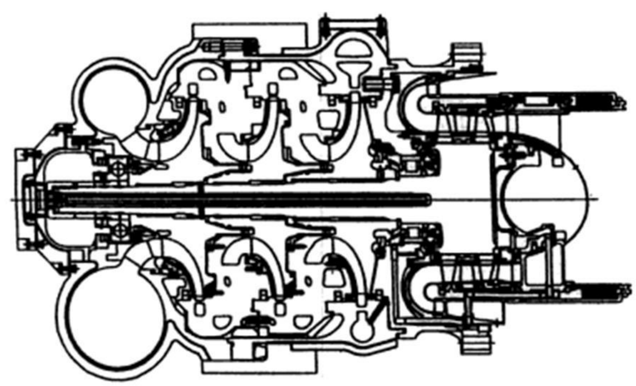

Figure 6. Space Shuttle Main Engine-High Pressure Fuel Turbopump (SSME-HPFTP).

Table 1. Summary of stability results of industrial example rotors employing a LeBlanc Balancer.

										Threshold speed of instability [rpm]					
								Rotor Internal		Loose		Tight			
Rotor	Direction	Operating speed [rpm]	Balance ring	K	Modal mass [kg]	Critical Speed [rpm]	Whirl frequency [cpm]	Loose	Tight	ωd op [rpm]	% of increase	ωd op [rpm]	% of increase	qm op [N/cm]	% of increase
Light rotor	Horizontal	Above critical	Without	3.4	215	5100	3735	0.059	0.0313	5148	4	6398	6	21390	12
			2				3776			5377		6794		24244	
	Vertical		Without	5.9			4912	0.059	0.0313	7928	5	10597	7	42749	11
			2				4990			8381		11382		48056	
Heavy rotor	Symmetrical	Above critical	Without	29.2	2524	2540	2519	0.059	0.0313	2872	1	3185	1	29320	4
			2				2522			2890		3216		30521	
8-stage compressor	Horizontal	10,000	Without	10.2	306	3821	3735	0.059	0.0313	5148	4	6398	6	21390	12
			2				3776			5377		6794		24244	
	Vertical		Without	0.36			3038	0.059	0.0313	12505	3	20883	3	143313	3
			2				3088			12853		21494		147815	
SSME-HPFTP	Symmetrical	28000	Without	0.71	29	16500	13880	0.118	0.0626	31076	21	46295	23	213187	27
			2				15903			39450		60290		291923	
			Without	2.02			15072	0.118	0.0626	25646	22	35004	26	131085	34
			2				16954			32946		47099		198260	
			Without	4.04			15660	0.118	0.0626	22243	23	28069	29	81610	43
			2				17478			29051		39293		143471	

A balance ring with dimensions r_o = 0.102 m (4 in), r_i = 0.076 m (3 in), h = 0.076 m (3 in), filled with a liquid density of ρ = 1300 kg/m^3 at ratio of 0.5 as recommend by [16] to maximize the balancing capabilities of the trapped fluid in the cavity. The fluid free surface radius r_f is given by Eq. (20).

$$r_f = \left[0.5\ \left(r_i^2 - r_o^2\right) + r_o^2\right]^{0.5} \tag{20}$$

Table 1 summarizes the threshold speed of instability and maximum aerodynamic cross-coupling improvements for all the example rotors.

DISCUSSION

The optimum bearing damping for all the rotors exemplified was determined and used as an input in the analysis. Despite of the optimization of the external damping and the relatively high internal rotor damping values employed significant improvements in the threshold speed of instability and maximum aerodynamic cross-coupling were obtained. However for the “heavy rotor” case, with the extremely stiff bearings, the flexible bearing critical speed is very close to the rigid bearing critical speed and even the external damping provided by the balance ring has little stabilizing effect since the bearing amplitudes are very small. The 8-stage centrifugal compressor with K = 0.36 in the vertical direction is another situation where the balance ring does not contribute much to the stability characteristics. In this case, the bearing supports flexibility is so large, that the external damping provided by the tilting pad journal bearings in series with the squeeze film dampers, is successful to provide enough damping to move forward the threshold speed of instability. The balance ring is of great help in the case of the SSME-HPFTP rotor, the internal rotor damping values used in this example are twice those for the other cases though. The apparent benefit is due to the high operating speed. This will need further experimental verification to ascertain whether the fluid behaves entirely as a solid at such high speed and confirm if the fluid backward traveling wave that provide the damping effect persists or vanishes.

The added mass of the balance ring was only 1.845 kg, the dimensions of the ring are feasible and relatively easy to fit in the rotors design with some engineering work. This kind of devices can be particularly attractive for using in hollow rotors. Note that the balance ring will show even better stability improvements in rotors that by design do not have optimum external damping. The analysis can be further extended to consider asymmetric and orthotropic supports and other models for internal damping available in the literature.

CONCLUSIONS

Built-up rotors are prone to instability due to internal damping. The assembly interface causes internal friction to arise. Some turbomachines account with shrink-fit aluminum wheels that may be potential sources of instability. In many other cases separating steel wheels and sleeves in between stages also interference fitted can add internal rotor damping. This paper presents for the first time the stabilizing capabilities of the LeBlanc balancer. Hollow rotors with fluid trapped inside, suspension segregation centrifuges, liquid-cooled gas turbines, spin-stabilized satellites, spinning rockets containing liquid fuel, home appliances such as washer machines, liquid-filled flywheel apparatus for motorcycles, automobiles, trailers and heavy vehicles tires self-balancing are just few examples of machines for which this kind of balancer is applicable not only to balance the rotating system but also to achieve much higher stable rotational speeds.

ACKNOWLEDGEMENTS

Thanks to Universidad Nacional Autónoma de México (UNAM) and the Consejo Nacional de Ciencia y Tecnología (Proyecto SEP-CONACYT-Ciencia Básica No. 83239) for granting support for presenting this paper.

REFERENCES

[1] Newkirk, B. L., 1924, "Shaft Whipping," General Electric Review, 27(3), 169-178.

[2] Kimball, A. L. Jr., 1924, "Internal Friction Theory of Shaft Whirling," General Electric Review, 27(4), 244-251.

[3] Gunter, E. J., 1966, "Dynamic Stability of Rotor-Bearing Systems," NASA Technical Report, SP-113.

[4] Black, H.F., 1976, "The Stabilizing Capacity of Bearings for Flexible Rotors with Hysteresis," *ASME Journal of Engineering for Industry*, (2) 87-91.

[5] Lund, J. W., 1986, "Destabilization of Rotors from Friction in Internal Joints with Micro-slip," International Conference in Rotordynamics, JSME, 487-491.

[6] Srinivasan, A., 2003, "The Influence of Internal Friction on Rotordynamic Instability," M.S. Thesis, Texas A&M University, May.

[7] LeBlanc, M., 1914, "Automatic Balancer for Rotating Bodies," US Patent 1,159,052.

[8] Ehrich, E. F., 1967, "The Influence of Trapped Fluids on High Speed Rotor Vibration," *ASME Journal of Engineering for Industry*, (89) 806–812.

[9] Hendricks, S. L., and Morton, J. B., 1979, "Stability of a Rotor Partially Filled With a Viscous Incompressible Fluid," ASME Paper 79-WA/APM-28, (48) 97-106.

[10] Hosoi, A., E., and Mahadevan, L., 1999, "Axial Instability of a Free-Surface Front in a Partially Filled Horizontal Rotating Cylinder," *Journal of Physics of Fluids*, (11-1), 97-106.

[11] Changsheng, Z., 2006, "Experimental Investigation Into the Effect of Fluid Viscosity on Instability of an Over-hung Flexible Rotor Partially Filled with Liquid", *ASME Journal of Vibrations and Acoustics*, 128, 1-10.

[12] Urbiola-Soto, L., and Lopez-Parra, M., "Dynamic Performance Of The LeBlanc Balancer For Automatic Washing Machines," ASME paper VIB-10-1123, *ASME Journal of Vibrations and Acoustics*, approved for production.

[13] Ehrich, F., and Childs, D., 194, "Identification and Avoidance of Instabilities in High Performance Turbomachinery," *Mechanical Engineering*, 66-79.

[14] Miles, J. W., and Troesch, B. A., 1961, "Surface Oscillations of a Rotating Liquid," *Journal of Applied Mechanics*," (28), 491–496.

[15] Barret, L. E., Gunter, E. J., and Allaire, P. E., 1978, "Optimum Bearing and Support Damping for Unbalance Response and Stability of Rotating Machinery," *ASME Journal of Engineering for Power*, (2) 89-94.

[16] Childs, D., 1993, Turbomachinery Rotordynamics: Phenomena, Modeling, and Analysis, John Wiley and Sons, New York.

APPENDIX 1- DERIVATION OF DISTANCE FROM FLUID C.G. TO POINTS C AND O

Assuming the fluid center of gravity **F** to be coincident with its centroid, the distance of the former to **C** is obtained according to

$$d = \frac{\Sigma C_n A_n}{\Sigma A_n} = \frac{(0)\pi r_o^2 - (-z)\pi r_f^2}{\pi(r_o^2 - r_f^2)} = z\frac{r_f^2}{r_o^2 - r_f^2}$$

Where n stands for the n-esim area A_n which centroid is at a distance C_n to the point **C**.

Similarly, the distance of the fluid center of gravity to **O** is given by

$$\bar{z} = \frac{\Sigma C_n A_n}{\Sigma A_n} = \frac{z_i \pi r_o^2 - (0)\pi r_f^2}{\pi(r_o^2 - r_f^2)} = z\frac{r_o^2}{r_o^2 - r_f^2}$$

Note that by employing d and $\bar{z}$ as expressed above, Eqs. (5) and (15) are put in terms solely of z and its derivatives, such that easily solvable second order ordinary linear differential equations with constant coefficients are obtained. The terms d and $\bar{z}$ are further useful substitution to simplify both, the unbalance response solution shown in Eq. (6), and the characteristic polynomial stated in Eq. (16).

APPENDIX 2- SIMPLIFICATION OF EQUATION OF MOTION

The differential equations of motion of a Jeffcott rotor mounted on symmetric flexible bearings are given by Eqs. (3) and (4).

Dividing Eq.(3) by m_r and since $\omega_{cr}{}^2 = k_r/m_r$

$$\ddot{\boldsymbol{z}} + \omega_{cr}^2(\boldsymbol{z} - \boldsymbol{z}_1) + \mathrm{M}\bar{\boldsymbol{z}}\omega^2 + 2\mathrm{M}_b\dot{\boldsymbol{d}}\omega = u\omega^2 e^{j\omega t} \qquad (21)$$

Similarly, Eq. (4) renders Eq. (22).

$$\frac{k_1}{m_r}\boldsymbol{z}_1 + \omega_{cr}^2(\boldsymbol{z}_1 - \boldsymbol{z}) + \frac{c_1}{m_r}\dot{\boldsymbol{z}}_1 = 0 \qquad (22)$$

Since K = k_1/k_r and $\xi_1 = c_1/2m_r\omega_{cr}$

$$2\omega_{cr}\xi_1\dot{\boldsymbol{z}}_1 + \mathrm{K}\omega_{cr}^2\boldsymbol{z}_1 + \omega_{cr}^2(\boldsymbol{z}_1 - \boldsymbol{z}) = 0$$

Assuming particular function solutions of the form $\boldsymbol{z} = ze^{j\omega t}$ and $\boldsymbol{z}_1 = z_1 e^{j\omega t}$ and dividing by $\omega_{cr}{}^2$

$$2j\xi_1 z_1 \mathrm{f} + \mathrm{K} z_1 + z_1 - z = 0$$

Rearranging and solving for $\boldsymbol{z}_1$ in terms of $\boldsymbol{z}$.

$$z_1 = \frac{z}{\left[\mathrm{K}+1+2j\xi_1\mathrm{f}\right]}$$

Multiplying by the complex conjugate in the numerator and denominator

$$z_1 = z\frac{\mathrm{K}+1-2j\xi_1\mathrm{f}}{(\mathrm{K}+1)^2+(2\xi_1\mathrm{f})^2}$$

Let D = $(\mathrm{K}+1)^2 + (2\xi_1\mathrm{f}\,)^2$, then

$$\boldsymbol{z}_1 = \frac{\mathrm{K}+1}{\mathrm{D}}\boldsymbol{z} - \frac{2\xi_1}{\mathrm{D}\omega_{cr}}\dot{\boldsymbol{z}} \qquad (23)$$

Substitution of Eq. (23) into Eq. (21) delivers

$$\ddot{\boldsymbol{z}} + \omega_{cr}^2\left\lfloor \boldsymbol{z} - \frac{\mathrm{K}+1}{\mathrm{D}}\boldsymbol{z} + \frac{2\xi_1}{\mathrm{D}\omega_{cr}}\dot{\boldsymbol{z}}\right\rfloor + \mathrm{M}\bar{\boldsymbol{z}}\omega^2 + 2\mathrm{M}_b\dot{\boldsymbol{d}}\omega = u\omega^2 e^{j\omega t}$$

$$\ddot{\boldsymbol{z}} + 2\omega_{cr}\frac{\xi_1}{\mathrm{D}}\dot{\boldsymbol{z}} + \omega_{cr}^2\left\lfloor 1 - \frac{\mathrm{K}+1}{\mathrm{D}}\right\rfloor\boldsymbol{z} + \mathrm{M}\bar{\boldsymbol{z}}\omega^2 + 2\mathrm{M}_b\dot{\boldsymbol{d}}\omega^2 = u\omega^2 e^{j\omega t}$$

Which with further algebraic manipulation reduces to

$$\ddot{\boldsymbol{z}} + 2\omega_{cr}\xi_e\dot{\boldsymbol{z}} + 2\mathrm{M}_b\dot{\boldsymbol{d}}\omega + \Omega^2\boldsymbol{z} + \mathrm{M}\bar{\boldsymbol{z}}\omega^2 = u\omega^2 e^{j\omega t}$$

The latest has the form of Eq. (5)